Aerosol Science and Technology, 38:588–597, 2004

ISSN: 0278-6826 print / 1521-7388 online
DOI: 10.1080/02786820490479897

Carbon Dioxide Uptake by Hydrated Lime Aerosol Particles

Biaohua Chen, Mary L. Laucks, and E. James Davis
Department of Chemical Engineering, University of Washington, Seattle, Washington

The reaction of the greenhouse gas, CO_2, with $Ca(OH)_2$ was explored using single-particle Raman spectroscopy to track the chemical reaction. Single particles were levitated in an electrodynamic balance (EDB) to maintain the particle in a laser beam. The levitation voltage provided gravimetric data. The humidity in the EDB chamber was varied to determine the effects of humidity on the reaction. It is demonstrated that no appreciable reaction occurs at low relative humidities ($RH < 70\%$). This is evidenced by no disappearance of the Raman peak associated with the $[OH]^-$ vibrational bond, but at high humidities ($RH > 70\%$) the Raman spectrum of $CaCO_3$ developed as the reaction proceeded. The results are consistent with results from packed-bed studies of the reaction and are in agreement with similar findings for the $SO_2/Ca(OH)_2$ reaction used for desulfurization, that is, the reaction does not proceed until multiple monolayers of water are adsorbed on the particle surface.

INTRODUCTION

More than a century ago Arrhenius (1896) recognized the possibility of global warming due to an increase in "carbonic acid" in the air. Mahlman and Stouffer (2002) reviewed the projection of future climate changes associated with CO_2 and other greenhouse gases. Although the natural production of CO_2 far exceeds that produced by human activity, the rate of increase is largely the result of man. A significant source of CO_2 related to human activity is the combustion of fossil fuels, and high-sulfur coal combustion has the combined problems of the generation of CO_2 as well as SO_2. Recently Lackner (2003) considered a variety of possibilities for CO_2 sequestration, one of which is the capture of CO_2 on lime.

An environmental problem associated with coal combustion is the formation of SO_2, and considerable work has been reported on the desulfurization of flue gas from coal-fired power plants. The Coolside process of the Consolidated Coal Company (Stouffer et al. 1989) involves spraying $Ca(OH)_2$ slurries into the flue gas followed by humidification with a water spray. In some cases NaOH is added to the water to enhance the SO_2 removal (1988). In field tests of the Coolside process with a 1-MW power plant in 1984 (Yoon et al. 1985a,b) up to 80% of the SO_2 was removed across the humidifier and the electrostatic precipitator (ESP) using hydrated lime and NaOH as an additive. The recently completed St. Johns River coal-fired power plant in Florida uses the hydrated lime process to remove SO_2 (*New York Times*, August 27, 2002). Using a pilot-scale test facility, Stouffer et al. (1989) clearly showed that SO_2 removal increased significantly with humidity. Based on water vapor adsorption measurements made by Klingspor (1983) and their SO_2 removal data, Stouffer and his associates concluded that "this result suggests that the SO_2 capture by $Ca(OH)_2$ requires at least one molecular layer of adsorbed water on the lime surfaces." Stouffer et al. (1989) also concluded that "The observed SO_2 removal was proportional to the number of layers of moisture that could physically adsorb on lime at equilibrium with humid flue gas."

A possible issue in the use of $Ca(OH)_2$ to remove SO_2 is that it can also remove CO_2 from the flue gas, and there is evidence that the $CO_2/Ca(OH)_2$ reaction also requires the uptake of water to have reaction. If there is significant uptake of CO_2 by the hydrated lime, the consumption of the reactant must be increased to remove the SO_2 as well as CO_2. There can be an advantage in the sequestration of CO_2 by hydrated lime in a regional sense, but there appears to be no global advantage because the hydrated lime is usually produced by heating limestone, $CaCO_3$, to form CaO, followed by the hydration of CaO, that is, by the reactions

$$CaCO_3 + \text{heat} \rightarrow CaO + CO_2, \quad [1]$$

$$CaO + H_2O \rightarrow Ca(OH)_2. \quad [2]$$

However, if the first reaction can be carried out at a site where the CO_2 can be sequestered in coal seams, salt mines, or other geological sinks, it would be feasible to use hydrated lime for CO_2 sequestration at fossil fuel power plants.

Using a packed-bed reactor, Beruto and Botter (2000) showed that the reaction of CO_2 with $Ca(OH)_2$ has many of the

Received 29 December 2003; accepted 29 April 2004.
Biaohua Chen is a visiting Scholar from Beijing University of Chemical Technology.
The authors wish to thank the National Science Foundation for Grant Number CTS-9982413 and the Chinese Scholarship Council for financial support.
Address correspondence to E. James Davis, Department of Chemical Engineering, Box 351750, University of Washington, Seattle, WA 98195-1750, USA. E-mail: davis@cheme.washington.edu

characteristics of the reaction between SO_2 and $Ca(OH)_2$ in that the reaction does not proceed at low relative humidities (RHs), but at high RHs the adsorption of water vapor on the particle surface leads to the formation of $CaCO_3$. Beruto and Botter concluded that multilayer adsorption yields a liquid-like interface in which Ca^{2+} and OH^- ions are formed as a result of the solubility of $Ca(OH)_2$ in the adsorbed phase. Since $Ca(OH)_2$ is only slightly soluble in water, scrubbing systems such as the Coolside process use an aqueous slurry of the hydroxide.

Adsorption isotherms of water vapor at 293 K for $Ca(OH)_2$ and $CaCO_3$ reported by Beruto and Botter are presented in Figure 1. These show that for RH > 70% the adsorption increases significantly as RH increases. For RH = 80% they estimated the number of water layers adsorbed on $Ca(OH)_2$ to be ~4 and on $CaCO_3$ ~ 2.6. They considered the reaction to follow the sequence of equations given by

$$CO_2(g) + H_2O(ads) \rightarrow H_2CO_3, \quad [3]$$

$$H_2CO_3 \rightarrow H^+ + HCO_3^-, \quad [4]$$

$$HCO_3^- \rightarrow H^+ + CO_3^{2-}, \quad [5]$$

$$Ca(OH)_2(s) \rightarrow Ca^{2+} + 2OH^-, \quad [6]$$

$$2OH^- + 2H^+ \rightarrow 2H_2O(ads), \quad [7]$$

$$Ca^{2+} + CO_3^{2-} \rightarrow CaCO_3(s). \quad [8]$$

The overall reaction is

$$Ca(OH)_2(s) + CO_2(g) \rightarrow CaCO_3(s) + H_2O(ads). \quad [9]$$

Here g refers to the gas phase, s to a solid phase, and ads to liquid-like phases (multilayer adsorbed water).

Beruto and Botter used mercury porosimetry to determine the pore size distribution of their powders. The bimodal distribution showed that most of the pore volume was associated with cavities between particles, and a much smaller fraction could be attributed to internal pores. Since the bulk of water could be in the interstices between particles in the packed bed, CO_2 could have dissolved and reacted in the interstitial water as well as with the adsorbed water. Particle–particle interactions in a packed bed

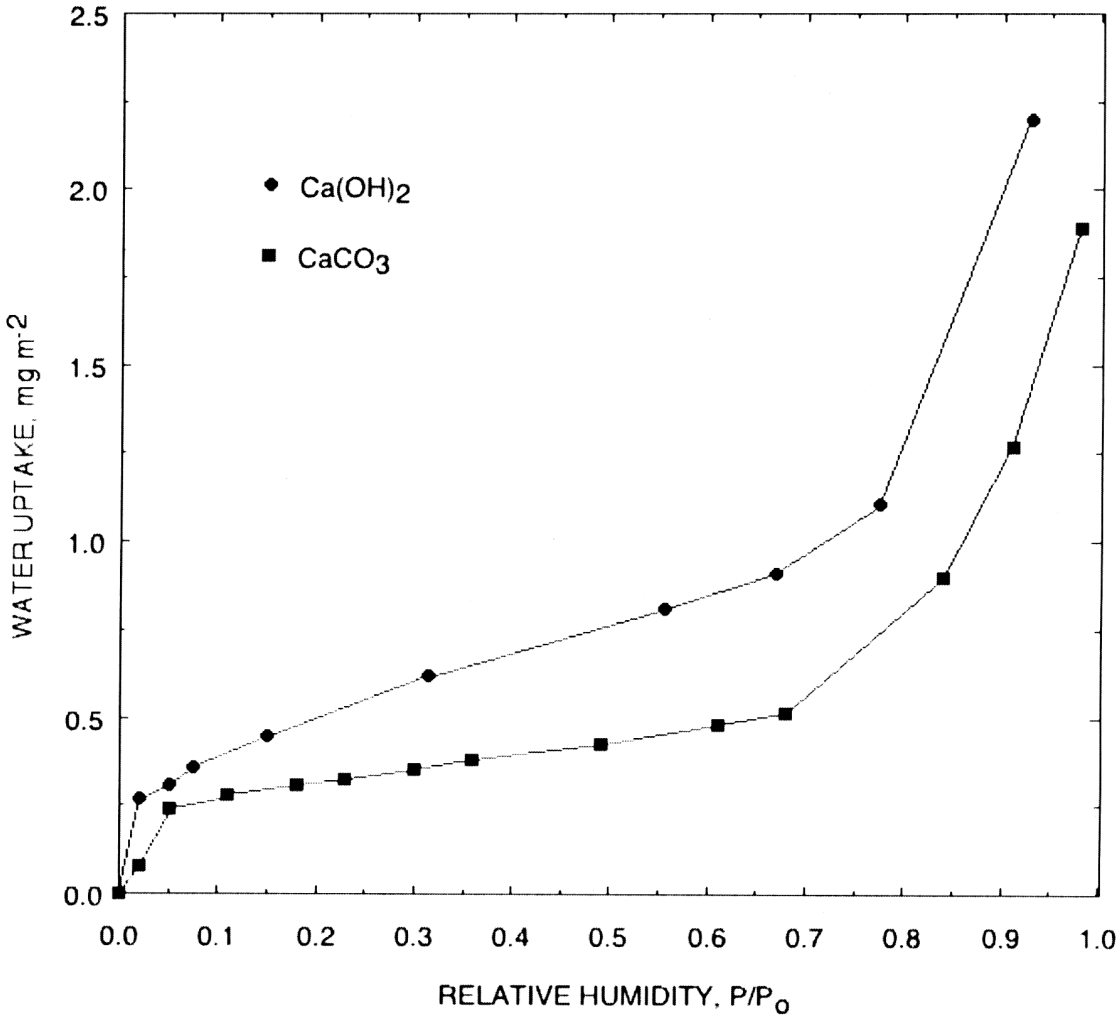

Figure 1. Adsorption isotherms for $Ca(OH)_2$ and $CaCO_3$ reported by Beruto and Bottter (2000).

do not occur in particles introduced into a flue gas by a spray, so we undertook a series of experiments to explore single particles levitated electrodynamically in a gas stream using Raman spectroscopy to follow the reaction.

The objectives were to determine the conditions (humidities) under which the gas–particle reaction proceeds, the extent of the reaction, and the possibility of pore plugging that prevents reaction. Pore plugging, particle coating, or both by the product is known to occur in the reaction between SO_2 and CaO (Rassat and Davis 1992). The molar volumes of $CaCO_3$ and $Ca(OH)_2$ are 0.0342 m^3 $kmol^{-1}$ and 0.0331 m^3 $kmol^{-1}$, respectively, so it is possible for pore plugging to occur as the hydroxide reacts to form the carbonate.

APPARATUS AND PROCEDURES

Figure 2 is an overhead photo of the experimental setup. A double-ring electrode configuration was used for electrodynamic containment of the particle, and the electrodes were mounted in a stainless steel chamber equipped with several viewing ports shown in the figure. Each electrode consisted of four segments to provide three-dimensional positioning of the particle by adjusting the dc potential on each segment. An ac potential of 2500 V was usually applied to both rings, and the ac frequency was usually 120 Hz. This octopole double ring electrodynamic balance (EDB) has been described in detail by Zheng et al. (2001), so only a brief description is given here.

Computer-controlled dc potentials were applied to the various segments to provide independent dc fields in the x, y, and z directions. By adjusting the dc potentials, the particle could be steered in the x and y directions. The x and y controls were necessary to balance lateral forces on the particle due to asymmetric radiation pressure of the laser beam, convection in the chamber, and any other lateral forces. The Z field balanced the gravitational force, the radiation pressure of the incident laser beam, and, if present, the aerodynamic drag force of the gas flow entering from below.

The EDB was optically coupled to the spectrometer system shown in Figure 3. As indicated in the figure, light scattered from the trapped particle at 90 degrees to the incident laser beam was collected through a lens in the EDB chamber, focused onto a pinhole, and then collimated. The collimated light passed through a Kaiser Optical Holographic notch filter (Super plus) for the 514.5 nm irradiation before being focused onto the slit of an

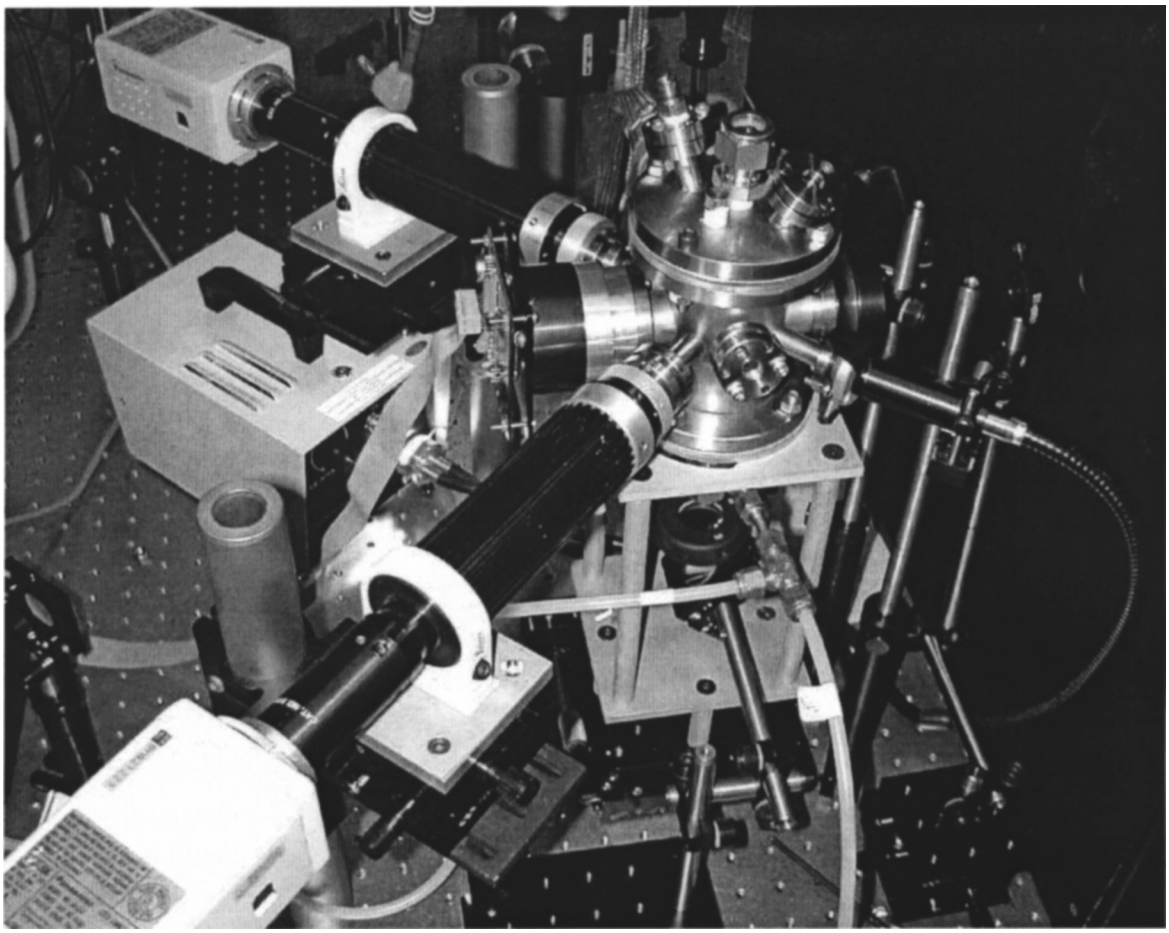

Figure 2. An overview of the electrodynamic balance and imaging systems.

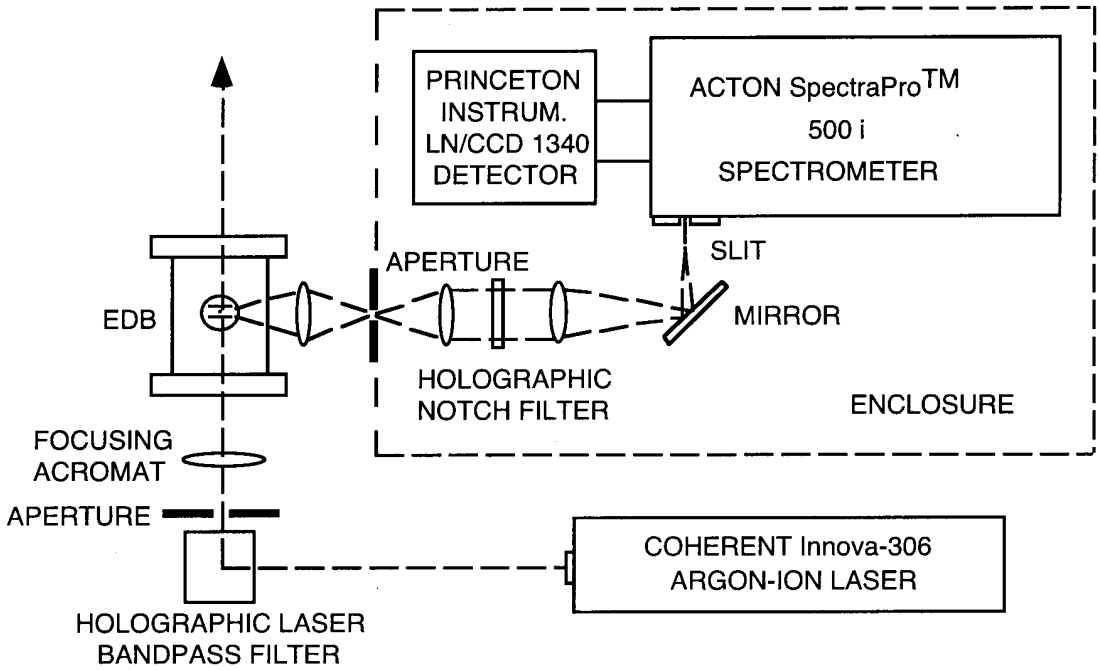

Figure 3. A schematic diagram of the experimental system.

Acton Spectra-Pro 500i spectrometer. A back-illuminated, liquid-nitrogen–cooled CCD camera (Princeton Instruments) was positioned at the exit focal plane of the spectrometer to record spectra. This single-monochromator system provides less light loss than double or triple monochromators at the cost of lower resolution.

Particle images from both x and y directions were acquired using two video cameras mounted outside observation ports of the EDB. The cameras and attached zoom lenses are shown in Figure 2. White light illuminated the trapped particle, and each video camera imaged the shadow of the particle. Each particle image was magnified by a factor of 9.45 with a zoom lens and displayed on a monitor. The total magnification of the particle image on the monitor was about 400×.

A particle was introduced into the balance chamber through one of the viewing ports on which was mounted a hinged window. A few particles were extracted from a powder sample kept in a dessicator by touching the powder with a hypodermic needle. The needle was then inserted into the chamber, and the high electric field near the rings induced a charge on the particles. A single particle was isolated by adjusting the ac field to eliminate all but one particle. The relevant principles of EDB particle trapping have been reviewed by Davis (1985) and Davis and Schweiger (2002).

The humidity in the chamber was adjusted by flowing dry CO_2 from a gas cylinder to a humidifier consisting of a glass condenser tube filled with glass beads. Water flowed down through the packed bed, and temperature-controlled water was circulated through the outer annulus of the condenser tube. The large surface area of the glass beads insured saturation of the gas at the exit of the humidifier. The humid stream was then brought to room temperature (293 K) before entering the EDB chamber. The humidifier provided RHs ranging from 20 to 90%, depending on the operating temperature of the condenser tube. The exit humidity was measured with a Vaisala humidity and temperature transmitter (Model HMP234) mounted in a tee connected to one port of the balance chamber, and after the particle was inserted the balance was sealed. Raman spectra were obtained as the chemical reaction proceeded, and the ratio of the particle mass to the initial mass was determined from levitation voltage measurements as discussed below.

In preliminary experiments gas flowed through the chamber during the measurements, but the gas flow destabilized the particle and made it difficult to obtain accurate gravimetric measurements. For the data presented here the particle existed in a stagnant gas during the period of data taking.

The particle weight, mg, is related to the dc levitation voltage, V_{dc}, by means of a force balance in the vertical direction,

$$mg = C_0 q V_{dc}/z_0 + F_{pr}, \qquad [10]$$

in which m is the particle mass, g is the acceleration of gravity, q is the Coulombic charge on the particle, C_0 and z_0 are geometrical constants that depend on the electrode configuration (see Davis and Schweiger 2002), and F_{pr} is radiation pressure force exerted by the laser beam. If the radiation pressure is sufficiently small, the particle mass is directly proportional to V_{dc}. The radiation pressure force was not always negligible, and the levitation voltages reported here are slightly affected by the radiation pressure. Since the radiation pressure depends on

the particle morphology, it varied somewhat due to particle rotation. The radiation pressure can be determined by measuring V_{dc} with and without the laser illumination, but such corrections were not made for the data reported here.

In principle, the absolute mass of a particle can be estimated by applying the stability characteristics of the EDB. Particle stability is governed by an ac field strength parameter, $\beta = 4q\,V_{ac}C_1/m\omega^2 z_0^2$, and an aerodynamic drag parameter, $\delta = 12\pi a\mu/m\omega$, in which V_{ac} is the ac levitation voltage, C_1 is a geometrical constant that depends on the electrode configuration, μ is the gas viscosity, and $\omega = 2\pi f$, where f is the ac frequency. Using Equation (10) with $F_{pr} = 0$, to determine q/m, the field strength parameter becomes $\beta = 4g\,(C_1/C_0)(V_{ac}/V_{dc})/\omega^2 z_0$. As indicated by Zheng et al. (2001), there is considerable uncertainty about the ratio C_1/C_0 based on three-dimensional (3D) simulations of the electric fields and oscillation measurements. Although this ratio can be determined by driving spheres of known size and density to instability (by varying V_{ac}, ω, or both), one cannot obtain reliable estimates of the particle mass for a nonspherical particle of unknown density by using this so-called springpoint method. Consequently, we followed the change in particle mass by recording the dc levitation voltage. If F_{pr} in Equation (10) is negligible compared with the particle weight, V_{dc} is directly proportional to the particle mass.

EXPERIMENTAL RESULTS

Particle Images

Figure 4 shows a sequence of images of a trapped particle obtained with the two video cameras during the course of an experiment in which humid CO_2 (RH = 81%) was present as the gas phase. The upper images were obtained at the beginning of the experiment, the middle pair at the maximum in the particle mass, and the bottom set at the end of the experiment. The particle is seen to be nonspherical, and initially the *y* axis dimension of the particle was approximately 21 μm. Although the particle mass changed significantly during an experiment, there were no major changes in the particle morphology (size changes).

Mass Changes

The levitation voltage for the particle shown in Figure 4 and for four other particles, plotted as $V_{dc} = |V_{dc}|$ versus time, are shown in Figure 5. The absolute value of the voltage is plotted because the particles could be positively or negatively charged, so V_{dc} could be negative or positive. Only the absolute value is needed to determine the particle mass. Since there is scatter in the voltage data due to the method of balancing the particle, each data point in Figure 5 represents the average of three consecutive voltages to reduce the scatter. The scatter arises

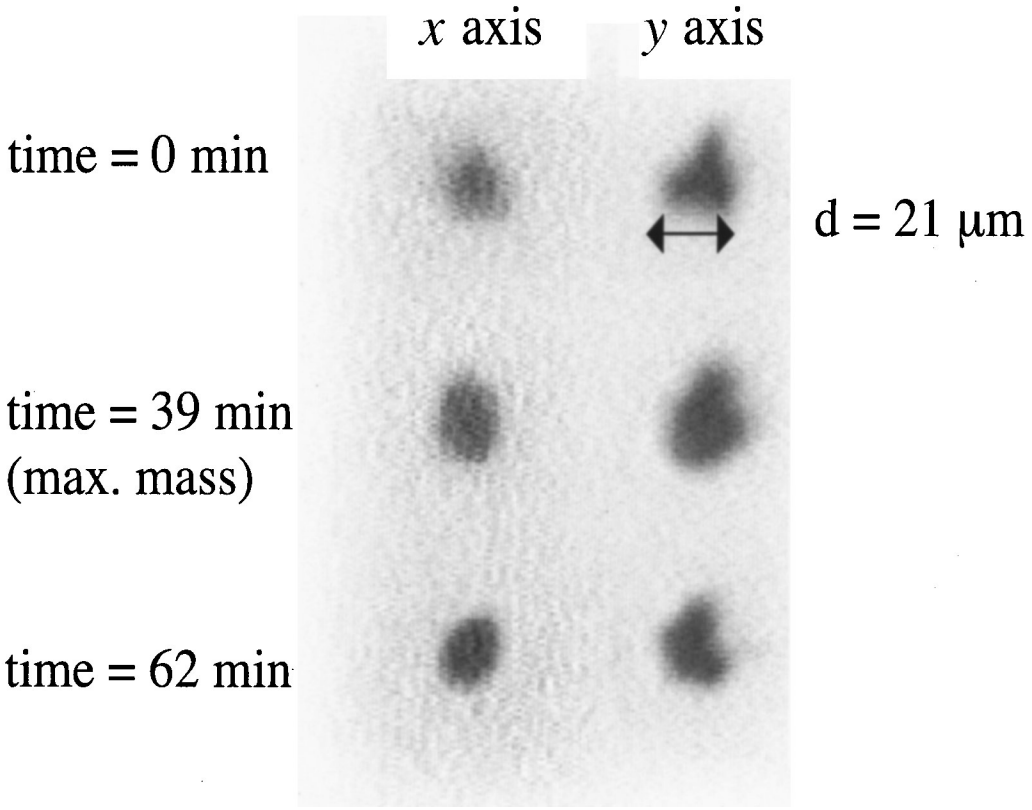

Figure 4. Images of a trapped particle during the course of reaction at an RH of 81%.

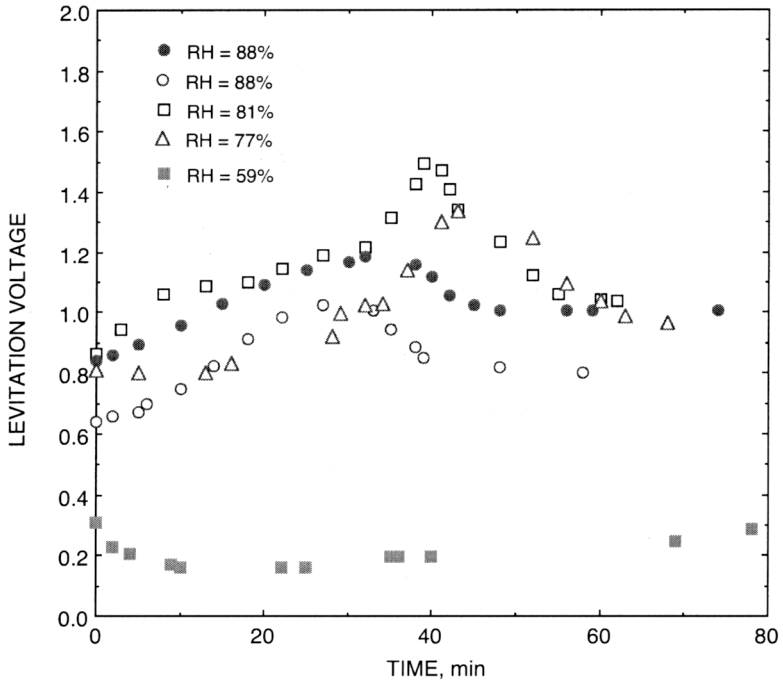

Figure 5. Levitation voltages as a function of time for particles reacting at various RHs.

because rotation of the nonspherical particle makes it difficult to maintain the particle exactly at the null point of the electrical field.

The data for RH = 59% are representative of data taken for RH < 70%, which show no significant reaction. The levitation voltage drifted downward and then returned to the initial voltage (within experimental error). This is substantially different from the results obtained at higher humidities for which the mass initially increased relatively slowly as water was adsorbed by the initially dry particle and the chemical reaction produced water within the particle. A maximum was reached, and the mass then decreased relatively rapidly. The decrease was due to the evaporative loss of water from the product, $CaCO_3$ (or $CaCO_3$ and unreacted $Ca(OH)_2$), as it equilibrated with the surrounding gas. This is qualitatively consistent with the water adsorption measurements of Beruto and Botter (2000). The adsorption isotherms reported by them for $CaCO_3$ and $Ca(OH)_2$ at 293 K and a relative humidity of 88% yield water uptake of 0.00102 g/m^2 for $CaCO_3$ and 0.00180 g/m^2 for $Ca(OH)_2$. Consequently, the water produced by the reaction in Equation (9) and some of the adsorbed water can be expected to evaporate.

The maximum voltage can be expected to correspond to a particle that has reacted to form $CaCO_3$ and H_2O. If the water produced by the reaction has been retained at that point in time and if the reaction has gone to completion, the ratio of the maximum voltage to the initial voltage should equal the stoichiometric ratio $(100.09 + 18.015)/74.09 = 1.594$. Similarly, if the final voltage corresponds to $CaCO_3$ containing a negligible amount of water, the ratio of the final voltage to the initial voltage should equal the stoichiometric ratio $100.09/74.09 = 1.351$. Table 1 lists the initial, V_0, maximum, V_{max}, and final, V_{final}, absolute voltages for the data shown in Figure 5. Also presented are the ratios V_{max}/V_0 and V_{final}/V_0, and the conversion calculated from the final voltage ratio.

The initial and final voltages were much easier to measure than the intermediate voltages because particle motion made it

Table 1
Voltages, voltage ratios, and conversions based on the final levitation voltages for the data of Figure 5

RH, %	V_0	V_{max}	V_{final}	V_{max}/V_0	V_{final}/V_0	% conversion
59	0.305		0.285		~1.0	~0
77	0.641	1.024 ± 0.031	0.801	1.598 ± 0.048	1.250	71
81	0.863	1.495 ± 0.062	1.039	1.732 ± 0.072	1.203	58
88	0.843	1.187 ± 0.006	1.007	1.408 ± 0.007	1.195	56
88	0.812	1.338 ± 0.129	0.968	1.648 ± 0.158	1.192	55

difficult to maintain the particle exactly at the nullpoint of the balance, and the rms errors for the maximum voltage are indicated in the table. That leads to uncertainty in the voltage ratio V_{max}/V_0. We note that some of the data for V_{max}/V_0 exceed the stoichiometric ratio 1.594. This reflects the inaccuracy associated with measuring V_{max}.

The mean values of the ratios V_{max}/V_0 and V_{final}/V_0 for the four data sets (for RH > 59%) presented in Table 1 are 1.597 and 1.210, respectively. The former is very close to the stoichiometric ratio 1.594, but the latter is lower than the stoichiometric ratio of calcium carbonate to calcium hydroxide. If the final state of a particle consists of $CaCO_3$, some unreacted $Ca(OH)_2$, and a negligibly small amount of adsorbed water, $V_{final}/V_0 = m_{final}/m_0 = 1.210$ corresponds to a 60% conversion of the hydroxide to carbonate. For the particles that reacted, the conversions calculated from the final voltages ranged from 55 to 71%, as shown in the table.

The mean value of the ratio V_{max}/V_0 ($\langle V_{max}/V_0 \rangle = 1.597$) suggests that the reaction went to completion, but the uncertainties in that voltage ratio make it difficult to conclude that the reaction went to completion. The measured ratios V_{final}/V_0 yield a significantly smaller conversion. The results based on the final voltages are more reliable those based on the maximum voltages, but this ambiguity cannot be definitively resolved here. The discrepancy cannot be attributed to charge loss by the particle, for charge loss would lead to a higher levitation voltage and larger calculated conversion. An increase in the Coulombic charge is most unlikely because there is no reasonable mechanism for an increase in charge.

Raman Spectra

The conversion of $Ca(OH)_2$ to carbonate by reaction with CO_2 involves the elimination of $[OH]^-$ bonds that have a Raman peak at ~3620 cm^{-1}. The $[OH]^-$ bonds in water adsorbed by the particle and water in the pores of a particle do not have such a sharply defined peak. Figure 6 shows Raman spectra for a single dry particle of $Ca(OH)_2$ and one that was exposed to water vapor at a humidity of 89 ± 1%. The $Ca(OH)_2$ was obtained from Sigma Chemical Co., St. Louis, MO, and kept dessicated until ready for injection into the balance chamber. As the particle took up water a broad fluorescence base developed in the Raman spectrum, and additional peaks appeared at 1348 cm^{-1} and 2853 cm^{-1}.

The formation of $CaCO_3$ can be followed using spectra in the region $\Delta\nu < 2000$ cm^{-1}. This is illustrated in Figure 7, which presents a spectrum for a dry levitated $CaCO_3$ particle and a calcite spectrum obtained from the literature (California Institute of Technology Division of Geological and Planetary Sciences). The carbonate sample was also purchased from Sigma Chemical Co. The spectrum of the calcium carbonate particle compares favorably with the CalTech spectrum, which has peaks at 281, 711, 1085, 1434, and 1748 cm^{-1}. The Raman spectrum of aragonite has many of the features of the calcite spectrum. Nakamoto (1986) reported vibrational frequencies of aragonite based on Raman measurements at 714, 1087, and 1432 cm^{-1}, and for CaO he reported 707 cm^{-1}. Thus, the peak at ~711 cm^{-1} can be attributed to the Ca—O bond.

Figure 8 shows a sequence of Raman spectra for a $Ca(OH)_2$ particle in CO_2 with a humidity of 59%. There is no significant

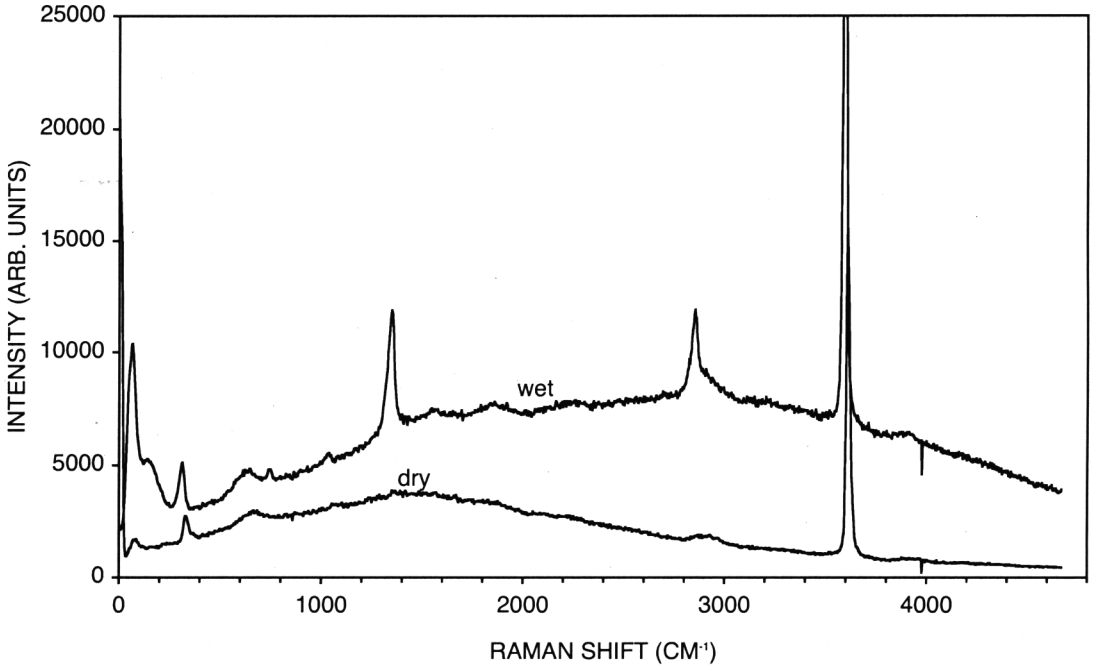

Figure 6. Raman spectra for a dry particle of $Ca(OH)_2$ and after exposure to a humidity of 89%.

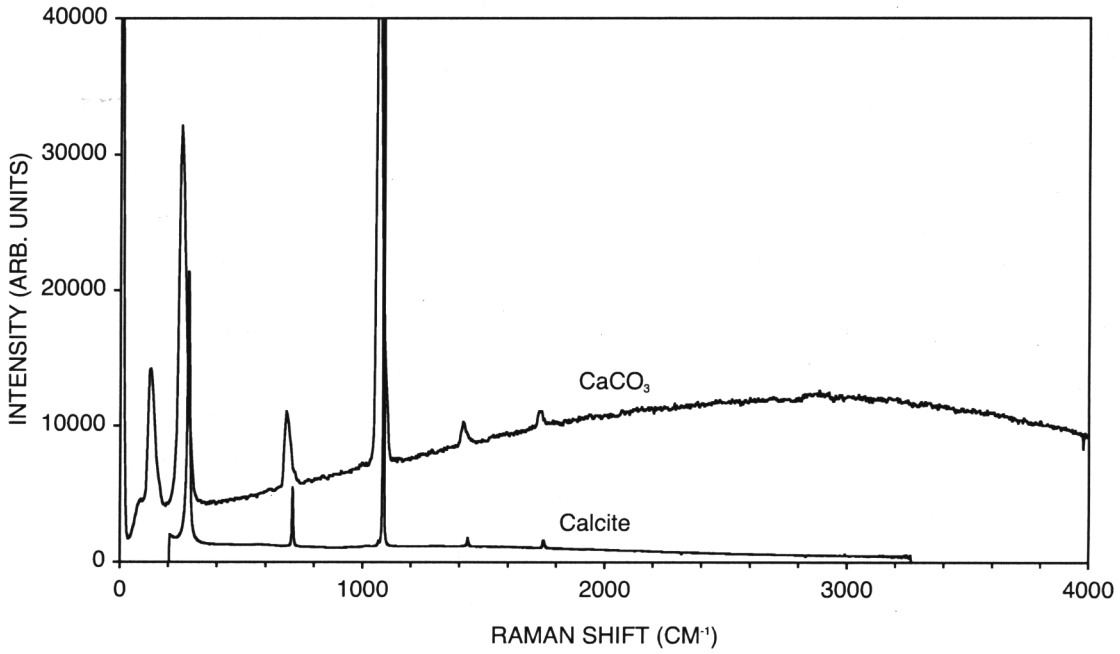

Figure 7. Raman spectra for a levitated $CaCO_3$ particle compared with the spectrum of calcite from the database of California Institute of Technology Division of Geological and Planetary Sciences.

decrease in the intensity of the Raman peak at $\sim$3620 cm^{-1}, but there is some indication of the formation of $CaCO_3$. No decrease in the key peak at 3620 cm^{-1} was observed at even longer times than indicated in the figure. This same result was observed for all experiments at low RH (RH $< 70\%$).

For higher humidities the effects of humidity on the process are illustrated in Figures 9 and 10, which show sequences of Raman spectra obtained in the sealed EDB chamber containing CO_2 at RH $= 76$ and 88%, respectively. The peak associated with the $[OH]^-$ bonds in $Ca(OH)_2$ is seen to decrease with time, and the peaks corresponding to $CaCO_3$ are seen to appear. The largest peak associated with $CaCO_3$ is at 1042 cm^{-1}, and it is clearly seen to increase as the peak at $\sim$3620 cm^{-1} decreases.

For these and numerous other experiments, it was observed that the $[OH]^-$ peak disappeared at the same time that the levitation voltage reached a maximum. Many experiments were

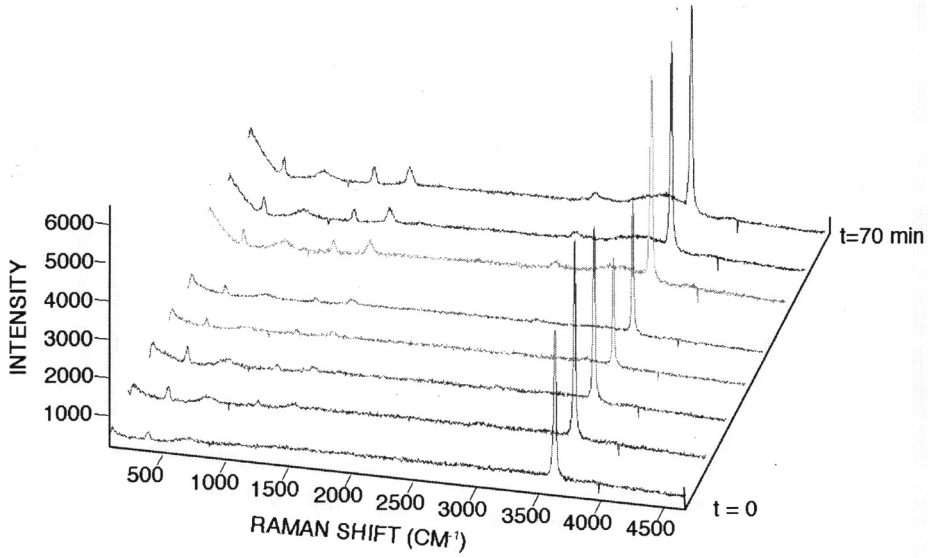

Figure 8. A sequence of Raman spectra for a lime particle reacting to exposure to CO_2 in the EDB chamber at an RH of 59%.

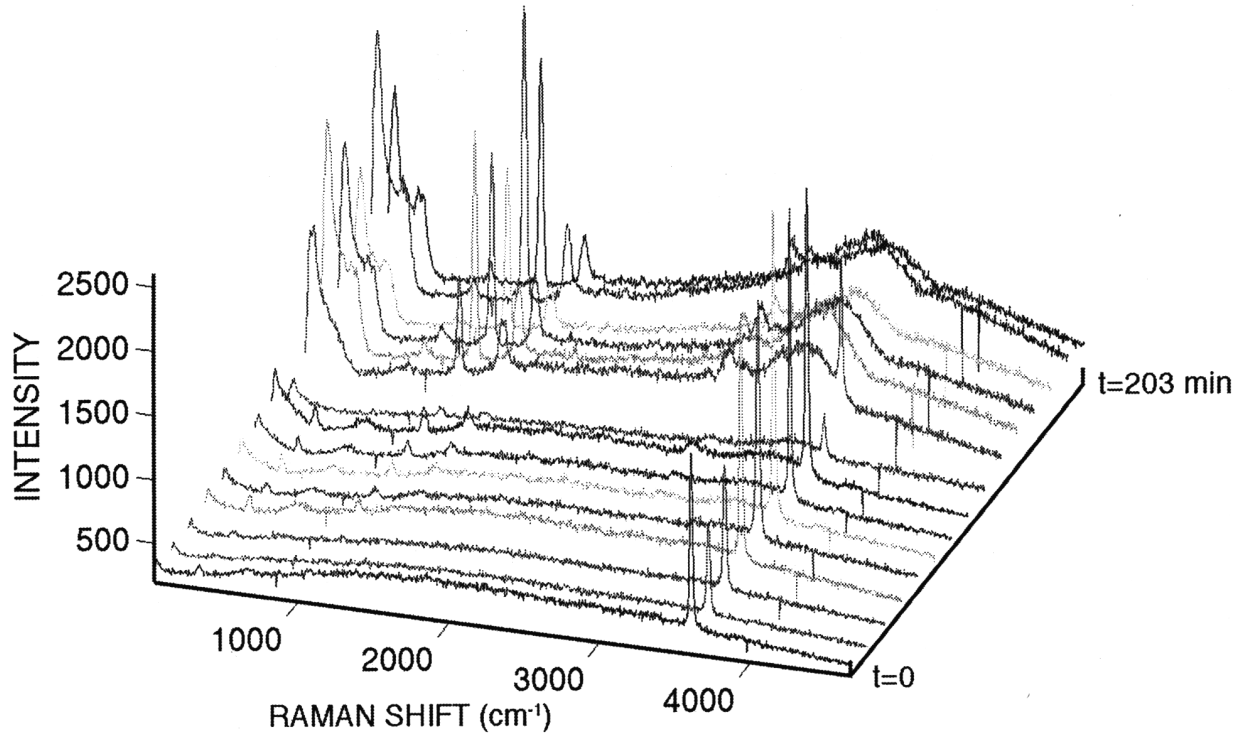

Figure 9. A sequence of Raman spectra for a lime particle reacting with CO_2 at an RH of 76%.

terminated when the particle became too unstable to obtain reliable voltage data.

DISCUSSION OF RESULTS

The relatively slow uptake of CO_2 at room temperature suggests that the process is rate controlled by internal diffusion and chemical reaction on a time scale of minutes. External mass transfer to or from the particle is a much more rapid process. For a spherical particle with radius a the steady-state mass flux of a gas phase species i is given by (Davis and Schweiger 2002)

$$j_i = \frac{D_{ij}M_i}{aRT}(p_a - p_\infty), \qquad [11]$$

in which D_{ij} is the diffusion coefficient of species i in carrier gas j, M_i is its molecular weight, R is the gas constant, T is the temperature, and p_a and p_∞ are the partial pressures of i at the gas–particle interface and far from the surface, respectively.

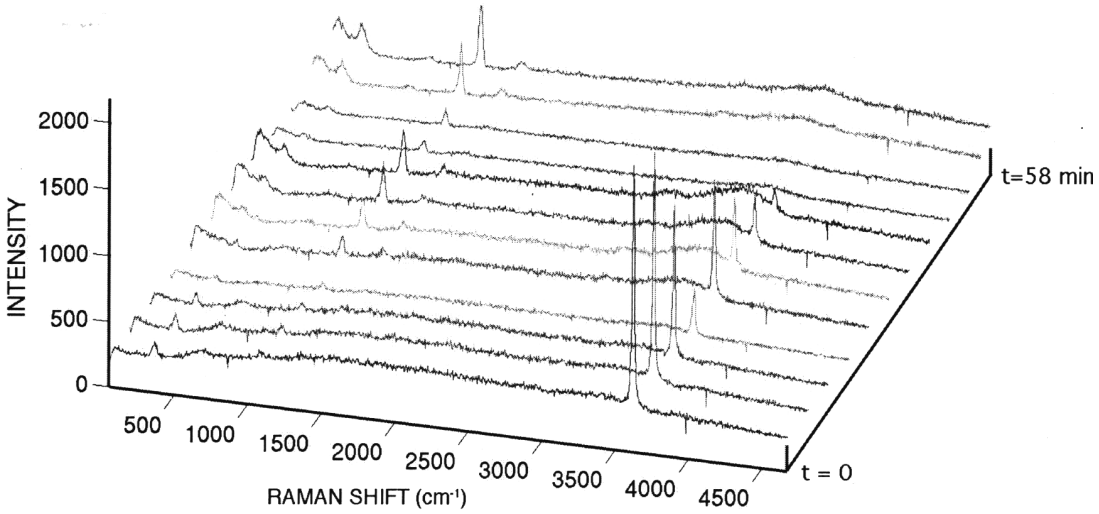

Figure 10. A sequence of Raman spectra for a lime particle reacting with CO_2 at an RH of 88%.

If the water formed by the reaction of CO_2 with $Ca(OH)_2$ evaporates isothermally at T = 293 K into the surrounding gas at a RH of 88%, the mass flux for a particle with a radius of 10.5 μm is given by

$$j_i = \frac{1.972 \times 10^{-5} \times 18.015(2339 - 2058)}{10.5 \times 10^{-6} \times 8314 \times 293} = 3.902 \times 10^{-3} \text{ kg m}^{-2} \text{ s}^{-1}, \quad [12]$$

where we assume that the interfacial partial pressure, p_a, is the vapor pressure of water (2.339 kPa) and $D_{ij} = 1.972 \times 10^{-5}$ m^2 s^{-1}. The rate of transport of water vapor to the surrounding gas is the product of the surface area and mass flux,

$$r_i = A_p j_i = 4\pi a^2 j_i = 5.41 \times 10^{-12} \text{ kg s}^{-1}, \quad [13]$$

Based on the data such as these in Table 1, if the initial mass of this particle is 1.08×10^{-11} kg (using 2240 kg m^{-3} for the density of $Ca(OH)_2$), then the maximum mass is 1.72×10^{-11} kg, and the final mass is 1.31×10^{-11}. Consequently, the water loss during the evaporation stage is 4.1×10^{-12} kg. At a constant rate of 5.41×10^{-12} kg s^{-1} the time required to transport the water from the particle to the gas phase is 0.8 s. This time scale is very much smaller than the time scale observed experimentally, which is on the order of 30 min.

These results suggest that the surface of the particle rapidly reaches equilibrium with the surrounding gas, and the rate of transport of water vapor and CO_2 into the particle is controlled by diffusion in the pores of the particle. From the results of Beruto and Botter it is likely that multilayer adsorption of water vapor occurs, the CO_2 and $Ca(OH)_2$ dissolve in the water, and reaction proceeds in the aqueous solution. The water generated in the reaction must then diffuse outward through the pores. The low solubility of $CaCO_3$ in water leads to precipitation of the carbonate.

The Raman spectra at larger times do not show the peak at 3620 cm^{-1} attributable to the $[OH]^-$ bond in the hydroxide, but it is not clearly established whether the Raman scattering from the core of the particle is detected. There could be unreacted $Ca(OH)_2$ in the core as suggested by the gravimetric data based on the final dc levitation voltages. The images taken during the course of reaction do not show an appreciable size change as the mass increased, which suggests that reaction occurred within pores of the particle. If the additional mass significantly changed the particle morphology, size, or both by reaction at the particle surface, we would have detected the change with our video camera setup.

One can expect the reaction to proceed much more rapidly at the higher temperatures of the Coolside process mentioned above, and if hydrated lime is used to remove SO_2 from a flue gas, there will be simultaneous reaction of SO_2 and CO_2 with the calcium hydroxide. The reaction with CO_2 requires additional hydrated lime compared with the requirement for only SO_2 removal. Because the CO_2 concentration (<20% by volume) of an exhaust gas is usually much higher than the SO_2 concentration (<2% by volume), the additional requirement of $Ca(OH)_2$ can be significant.

The results presented here could apply to the sequestration of CO_2. However, there is no global advantage if CO_2 is sequestered locally using hydrated lime unless the CO_2 produced by the reaction in Equation (1) can be sequestered at the site where the CaO is produced.

REFERENCES

Arrhenius, S. (1896). On the Influence of Carbonic Acid in the Air Upon the Temperature of the Ground, *London Edinburgh Dublin Philos. Mag. J. Sci.* 41:237–276.

Beruto, D. T., and Botter, R. (2000). Liquid-Like H_2O Adsorption Layers to Catalyze the $Ca(OH)_2/CO_2$ Solid-Gas Reaction and to Form a Non-Protective Solid Product Layer at 20°C, *J. European Ceramic Soc.* 20:497–503.

Davis, E. J. (1985). Electrodynamic Balance Stability Characteristics and Applications to the Study of Aerocolloidal Particles, *Langmuir* 1:379–387.

Davis, E. J., and Schweiger, G. (2002). *The Airborne Microparticle: Its Physics, Chemistry, Optics and Transport Phenomena*, Springer-Verlag, Heidelberg, Germany.

Klingspor, J. (1983). Kinetic and Engineering Aspects on the Wet-Dry FGD Process. Licenciate Thesis, Lund Institute of Technology, Lund, Sweden.

Lackner, K. S. (2003). A Guide to CO_2 Sequestration, *Science* 300:1677–1678.

Mahlman, J. D., and Stouffer, R. J. (2002). Projection of Future Changes in Climate, In *Encyclopedia of Gobal Environmental Change*, edited by T. Munn. Wiley, New York, pp. 126–138.

Nakamoto, K. (1986). *Infrared and Raman Spectra of Inorganic and Coordination Compounds*, 4th ed., John Wiley & Sons, New York.

New York Times. (2002). August 27.

Rassat, S. D., and Davis, E. J. (1992). Chemical Reaction Between Sulfur Dioxide and a Calcium Oxide Aerosol Particle, *J. Aerosol Sci.* 23:765–780.

Stouffer, M. R., Yoon, H., and Burke, F. P. (1989). An Investigation of the Mechanisms of Flue Gas Desulfurization by In-Duct Dry Sorbent Injection, *Ind. Chem. Res.* 28:20–27.

Yoon, H., Ring, P. A., and Burke, F. P. (1985a). Coolside SO_2 Abatement Technology: 1 MW Field Tests, In *Proc. Coal Technol. '85 Conf.*, Pittsburgh, PA.

Yoon, H., Stouffer, M. R., Rosenhoover, W. A., and Statnick, R. M. (1985b). Laboratory and Field Development of Coolside SO_2 Abatement Technology, In *Proc. 2nd Annual Pittsburgh Coal Conf.*, Pittsburgh, PA.

Yoon, H., Stouffer, M. R., Rosenhoover, W. A., Withum, J. A., and Burke, F. P. (1988). Pilot Process Variable Study of Coolside Desulfurization, *Environ. Prog.* 7:104–111.

Zheng, F., Qu, X., and Davis, E. J. (2001). Electrodynamic Balance with Octopole Double-Ring Electrodes for Three-Dimensional Force Compensation, *Rev. Sci. Instrum.* 72:3380–3385.